Eng. & Tech. Journal ,Vol.29, No. 14 , 2011

Validation of Numerical Computations and Turbulence Models Combinations for Gas Turbine Cascade Blade Flow

Dr.Assim Yousif Hameed* & Hakem Tarteb *

Received on: 10/6 /2010
Accepted on: 2 /6/2011

Abstract

The accuracy of computer codes for turbo-machinery turbulent flow field calculations relies strongly on the type and behavior of the turbulence model used in the computations**.** Analysis of different Reynolds Average Navier-Stokes Equation (RANS) based turbulence models was applied to predict the flow field in the linear first stage gas turbine cascade blade. The experimental investigation is also introduced to validate the accuracy of turbulence models. This was done by using five linear cascade blades tested in an open jet type low-speed subsonic wind tunnel. The static pressure distribution was measured at the midspan of cascade middle blade by using static pressure taps. The numerical results obtained from different turbulence model simulations is individually reviewed for the correctness of its predictions and compared with the experimental data in terms of integrated flow parameters, such as static pressure coefficient distribution on both blade sides. The results show that RNG k-ε turbulence model gave the best prediction of pressure distribution when compared with the experimental data. Prediction of standard k-ε and k-ω turbulence models fail to predict accurately the flow field parameters in cascade passage. Prediction of (k-ε) turbulence model overestimate the turbulence kinetic energy values, especially in the regions of high velocity at blade suction side, also not accurately predict the flow separation on the blade suction side.

Keywords: turbulence model, cascade, pressure coefficient, kinetic energy, dissipation

صلاحية مزاوجة الحل العددي مع نماذج الاضطراب لجريان خلال صف من ريش تربين غازي

الخلاصة

إن دقة البرمجيات والتجفيرات الحاسوبية المعدة لإجراء الحسابات في مجالات الجريان الاضطرابي للمحركات التربينية يتبع بقوة نوع وسلوك نموذج الاضطراب المستخدم في هذه الحسابات. تم تحليل متوسط رينولدز لمعادلات نفير وستوك للتنبؤ عن مجال الجريان في صف ريش المرحلة الأولى لتربين غازي. كذالك تم تقديم محاكاة للاختبارات التجريبية للكشف عن صلاحية ودقة المزاوجة بين الحل العددي ونماذج الاضطراب. اجريت التجارب في صف من الريش المستقيمة اختبرت في نفق الريح الواطيء السرعة ذي النفاث المفتوح. تم توزيع فتحات قياس الضغط في منتصف باع الريشة الوسطى لصف الريش. إن النتائج العددية المستحصلة لمختلف نماذج الاضطراب قد قدمت بشكل منفصل وتم مقارنتها مع المعطيات التجريبية بدلالة المعالم التكاملية للجريان مثل توزيع معاملات الضغط الستاتيكي على سطحي الريشة. بينت النتائج ان نموذج الاضطراب(RNG k-ε) عطى افضل تنبؤ لتوزيع الضغط عند مقارنتة مع المعطيات التجريبية. في حين فشلا نموذجي الاضطراب (k-ε) و (k-ω) في التنبؤ الدقيق لمجال الجريان في مجرى صف الريش بينما اعطى نموذج الاضطراب (k-ε) تخمين اعلى لقيم الطاقة الحركية

* Machines & Equipments Engineering Department, University of Technology/ Baghdad

الاضطرابية, لا سيما منطقة السرع العالية في سطح المص للريشة كما لم يعطي تنبؤ دقيق عن موقع انفصال الجريان عند هذا السطح.

1- Introduction

It is highly desirable to have a powerful, generalized turbulence model which accurately models the full range of turbulence effects across a wide range of common turbomachinery flows without substantial user interaction. The most computationally practical method of dealing with turbulence is by way of the Reynolds Averaged Navier-Stokes (RANS) equations. The goal of RANS turbulence modeling is to prescribe the correlation of the Reynolds stress tensor. Physically, the correlation is an artifact of Reynolds averaging the Navier-Stokes equations. It represents the time-averaged rate of turbulent momentum transfer **[1]**. There are several mainstream turbulence models of varying degrees of complexity. They can be classified by the number of extra partial differential (or transport) equations that must be solved (in addition to the conservation equations). Transport equations allow non-local and flow history effects to be included in the description of the local turbulence. The most simple turbulence models are algebraic or
Zero-equation models; they require no solution of differential Equations and therefore can only use information from local variables. There are also several prominent one and two equation turbulence models. The most complex class of turbulence models are Full Reynolds Stress Models (FRSM) with which each independent component of the Reynolds stress tensor is solved by a transport equation.

Literatures show many contributions in this field in which [2] studied a three-dimensional Navior-Stokes analyzer based on a control volume method developed to simulate the complex flow field within a turbomachinery. Turbulent stresses were approximated by modifying Baldwin-Lomax algebraic, k-e, R k-e and RNG k-e turbulence models. The applications of the computational modeling for the evaluation of three-dimensional compressible turbulent flow characteristics were focused by [3]. The calculations were performed with the use of Reynolds averaged Navier-Stokes (RANS) equations based turbulence models, namely the standard k-ε and k-ω turbulence models.

Comparison between the experimental and CFD (Computational Fluid Dynamics) data in so called a verification test were presented by [4]. The

experimental part includes measurements of static pressure distribution, measured at mid span of the blade. The flow regarded incompressible flow (M<0.2). Different turbulence models were used in this study such as, SST k-ω, k-ε, and RNG k-ε. Also [5] conducted 3D numerical simulations of turbulent incompressible flows validated against the experimental data from linear low pressure turbine/outlet guide vane cascade. Results from three different turbulence models as implemented in FLUENT, k-ε Realizable, SST k-ω and the Reynolds Stress Models were validated against detailed measurements.

At the present work the effect of several turbulent models has been used to predict the aerodynamics characteristic of two-dimensional turbulent flows through gas turbine cascade. Numerical simulations were performed on an irregular quadratic structured grid with the FLUENT (V6.3) software package which solves the Navier–Stokes equations by using finite volume methods. Two-dimensional stationary numerical simulations were made under turbulent conditions allow to compare the effect of flow characteristics through the cascade blade passage. Processor step of the solution **is** done by solving NAVIER-STOKES equations (continuity and momentum equations), and the turbulence flow model as implemented in FLUENT Cod. The computational results were examined with using five turbulence models available in the computational cod used to find the correctness of the CFD code prediction. These models are standard (k-ε), RNG (k-ε), realizable (k-ε) as R (k-ε), standard (k-ω) as S (k-ω) and SST (k-ω)). Each turbulence model was individually reviewed. Postprocessor step was done by reviewing the results of the computational code.

Experimental and numerical data were obtained at the cascade mid blade and at blade midspan. The predicted data is compared and analyzed with the similar data obtained from experimental work for the identical cascade blade. In experimental investigation test a cascade is tested in an open jet low speed wind tunnel. The blade profile that is used in measurements is of a first stage rotor of the high pressure (HP) turbine of the F-100-PW-220 military turbofan. The pressure distribution around the cascade blade midspan is measured. The remarkable differences in the five turbulence models used in the present predictions of C_P are discussed.

2-Experimental set-up

This was done by manufacturing five linear cascade blades tested in an open jet type low-speed subsonic wind tunnel. The static

pressure distribution at blade midspan was measured by using static pressure taps**.** The wind tunnel designed and constructed for purpose of the present experimental investigation. The operating velocity at the test section, in which the flow is incompressible, can be adjusted from (4m/s) to (35m/s). The flow velocity in the cascade entrance can be controlled by means of the electrical motor rotation (AC drive motor) and a double butterfly valve located at the wind tunnel inlet. Pitot – static tube is used to measure the air velocity inside the inlet cascade section. The Reynolds number based on the mean velocity of the wind tunnel test section and the blade chord length at the present investigation, the Reynolds number fixed at ($2x10^5$) for all the experimental investigation. The cascade is a row of linear two-dimensional blades having the same geometrically shape of real gas turbine blades. The cascade consisted of five blades each 135 mm of axial chord; the blade geometry is the same of a first stage rotor blade of the high pressure (HP) gas turbine of (F-100-PW-220 military turbofan}, in which it used as a power plant of the F-16 aircraft [6]. Figure (1) manifests the cascade arrangement of blade. All the dimensions and angles for this blade cascade can be found in table (1). The pressure coefficient presented in this work is defined as:

$$C_p = \frac{(p - P_\infty)}{1/2\rho U_\infty^2} \quad (1)$$

Where C_p represent the static pressure coefficient, p is the blade surface static pressure, P_∞ is the free upstream total pressure, ρ is the air density, and U_∞ is the free stream velocity measured just upstream the cascade.

To estimate the static pressure coefficient distributions, and in order to be convenient with the requirements of experimental accuracy, i.e. the effects of the wind tunnel test section walls, the middle blade in cascade is selected to do the static pressures measurements on both blade sides. Therefore, midspan region of the midblade provided with thirteen static pressure taps, first static pressure tap is located at the blade leading edge stagnation point, seven static pressure taps on the suction surface and five on the pressure surface. The surface pressure is transmitted through (0.7 mm) diameter that are molded inside the blade, care being taken to make the static holes flush to surface and to insure that holes are with right angles to surface to minimize the reading errors.

The condition, under which a model is tested in the test rig, is not the same as those in free air. The effects of the walls, the model thickness, and wake are subjected

to the solid and wake blocking. The maximum ratio of model frontal area to test cross-sectional area of 7.5 % should be probably used according [7]. In the present investigation, the cascade frontal area to the test cross-section area is less than 7.5 %. This means that the blocking errors are very small and may be neglected in which

3-Boundar condition and ssumption

In order to develop an applicable comprehensive computational method, some assumptions were made for the flow, and these are, steady two-dimensional incompressible fluid flow, the entering flow is subsonic everywhere, the fluid is Newtonian, the flow is viscous, the flow is isotropic and turbulent, the flow is isothermal, and neglecting the body forces. Pressure inlet boundary conditions are used to define the fluid pressure at flow inlet along with all other scalar properties of the flow. It's suitable for incompressible flow calculations. Pressure inlet boundary conditions can be used when the inlet pressure is known, but the flow rate and/or velocity is not known. It is useful to move the boundary as far from the region of interest as possible where the general flow is known. The total pressure for an incompressible fluid is defined as:

$$P_t = P_s + \frac{1}{2}\rho|\vec{u}|^2 \qquad (2)$$

Pressure outlet boundary conditions require the specification of a static (gauge) pressure at the outlet boundary.

Velocity inlet boundary conditions are used to define the flow velocity along with all relevant scalar properties of the flow, at flow inlets.

Turbulence quantities, ($\tilde{\nu}$), (k), (ε), and (ω) used in the turbulent models are normally not known, but they must be estimated as given by [8] as follows:

$$\tilde{\nu}_1 = \sqrt{\frac{3}{2}}\, u_{1I}\, L_C \qquad (3)$$

Where

(u_1) is the magnitude of velocity at cascade inlet.

(I) is the turbulence intensity, turbulence parameters, and its value ranging between ($0.01 \le I \le 0.1$), the correct values of (I) used according to the information given in[8].

(L_C) is the turbulence length scale, turbulence parameters, and is taken as (20% s), where (s) is the inlet height (cascade pitch) [9].

The kinetic energy is set to:

$$k_1 = \frac{3}{2}\,(I\,u_1)^2 \qquad (4)$$

The dissipation is set to:

$$\varepsilon_1 = C_\mu^{3/4}\,\frac{k_1^{3/2}}{L_C} \qquad (5)$$

Where C_μ is an empirical constant specified in the turbulence model, for standard k-ε model C_μ = 0.09, and for RNG k − ε model C_μ = 0.0854 which is derived from the RNG theory, and is very close to the empirical value of k-ε model 0.09.

The specific dissipation is set to:

$$\omega_1 = \frac{k_1^{1/2}}{C_\mu^{1/4} L_C} \quad (6)$$

(I) and (L_C) in equations (5) and (6) are called turbulence parameters.

4- Near wall treatment

The k-ε models are primarily valid for turbulent core flows (i.e., the flow in the regions somewhat far from walls). Therefore consideration needs to be given as to how to make these models suitable for wall-bounded flows. The Spalart-Allmaras and k-ω models are designed to be applied throughout the boundary layer, provided that the near-wall mesh resolution is sufficient. The near wall region is theoretically subdivided into three regions. The region closest to the wall, where the viscous forces dominate, and the flow is dominated by the molecular viscosity is called as the viscous sublayer. In the outermost region, the momentum dominates over viscosity, and hence the turbulent viscosity dominates. In the intermediate region, both the viscous forces and turbulence are equally important. Generally, one approach is used to model the near wall region, as given by [10], in which they gave standard wall functions and have been most widely used for industrial flows as a special formula for evaluating the effective exchange coefficient at the wall. Also [11] gave the expressions for the wall function for different dependent variables based on a dimensionless quantities andThe implementation of wall boundary conditions in turbulent flows starts with the evaluation of:

$$y^+ = \frac{y_p}{v}\sqrt{\frac{\tau_w}{\rho}} \quad (7)$$

$$v = \frac{\mu}{\rho} \quad (8)$$

$$\sqrt{\frac{\tau_w}{\rho}} = u_\tau \quad (9)$$

In equations (7) and (8),

Where v is represent the kinematic viscosity and u_τ the friction or shear velocity.

Equation (37) becomes:

$$y^+ = \frac{\rho\, y_p\, u_\tau}{\mu} \quad (10)$$

, or

$$y^+ = \frac{\rho\, C_\mu^{1/4} k_p^{1/2} y_p}{\mu} \quad (11)$$

y_p is the distance of the near wall node p to the solid surface. The wall shear stress is assumed to be entirely viscous in origin. If y^+>11.63 according to [11], the flow is turbulent, and the wall function approach is used.

The log-law of the wall for mean velocity yields:

$$u^+ = \frac{1}{\kappa} \ln(E y^+) \qquad (12)$$

In this formula, κ is von Karman's constant and taken equal to (0.4187) and *E* is an integration constant that depends on the roughness of the wall. For smooth walls, *E* has a value of (9.793) according to [12]. The node (p) is considered to be in the log-law region of a turbulent boundary layer. In this region, the wall function formulae associated with the log-law are used to calculate the shear stress [23].

5-Distribution of pressur Coefficients

Experimental and numerical static pressure coefficients distributions were obtained at the cascade mid blade and at blade midspan. These results are presented in figure (2).

Turbulence models are often judged for accuracy based on the comparison of their predictions with the experimentally observed values. The numerical pressure coefficient distributions showed scattered values upon the experimental results. The standard k- ε model and the standard k-ω model predict slightly high pressure coefficients values when compared with experimental values, but the difference between them is that the standard k-ω predicts high pressure coefficient at the nose and along the suction side, while it predicts low values for the residual part of pressure side. The SST k-ω model predicts the most negative pressure coefficients. The, S k-ε RNG k-ε and R k-ε predictions are very close to each other for both suction and pressure sides. RNG k-e model gave the most closeness prediction of pressure distribution when compared with the experimental data.

6-Distribution of turbulent kinetic energy

The accuracy of turbulence models is often associated with the estimation of turbulent kinetic energy in the flow. With known turbulent kinetic energy, *k* and dissipation rate ε, the turbulent viscosity is calculated as:

$$\mu_t = \rho C_\mu \frac{k^2}{\varepsilon} \qquad (13)$$

The production of *k* is an important parameter that affects the pressure distribution. High values of *k* are predicted near high velocity gradients, because of the production term in the transport equation for *k* which increases with increasing velocity gradients, and hence increasing shear in the flow. The turbulent kinetic energy distribution is presented as contours for different turbulence models, as shown in figure (3). Also, *k* distributions for these models on lower and upper sides of the blade are shown in figures (4, a,

& b). The standard k-ω model and the standard k- ε model predict relatively high values of turbulent kinetic energy; the standard k-ω shows interestingly high values of turbulent kinetic energy at the nose region. The RNG k- ε model distributions of k agree well with those of the R k- ε model. The SST k- ω predicts considerably low *k* values for both the suction and pressure sides due to the slow growth of shear stresses as shown in figures (5, a & b). As a matter of fact, the production of turbulent kinetic energy dominates in the regions of high shear and high velocity gradients. The turbulent kinetic energy is transferred from large eddies to small eddies in the turbulent flow. Eventually, the small eddies dissipate the energy received.

7-Distribution of the turbulence dissipationrate

The dissipation of energy is an important mechanism of conservation of energy in the turbulent flow. The rate of dissipation of this energy is measured in terms of the turbulence dissipation rate in the two-equation turbulence models.

The general trend turbulence dissipation rate of distribution is similar to the distribution of turbulent kinetic energy (k). The equilibrium between the production and dissipation of *k* is the feature of the RANS based turbulence models. The realizable k-ε model [14] does not have a production term in the transport ε equation, unlike other two k- ε models [9]. But, it predicts large dissipation rate similar to the RNG k- ε model. The RNG k-ε model [15] involves an extra term in the transport equation for the turbulence dissipation rate. The term R_ε is given by:

$$R_\varepsilon = \left[\frac{C_\mu \eta^3 \left(1-\eta/\eta_0\right)}{1+\beta\eta^3}\right] \rho \frac{\varepsilon^2}{k} \qquad (14)$$

Where

$$\eta \equiv \frac{sk}{\varepsilon}, \quad \eta_0 = 4.38, \quad and \quad \beta = 0.012 \qquad (15)$$

This term compared with the term $C_\mu \rho \frac{\varepsilon^2}{k}$ in equation (13), takes into account the effects of rapid strain in complex turbulent flows. i.e., when $\eta < \eta_0$, the R_ε term is positive, and it adds to the C_μ term resulting in similar predictions as that of standard k-ε. But, for highly strained flows where $\eta > \eta_0$, the R_ε term is negative and decreases the effective contribution from $\rho\varepsilon^2/k$, thus predicting lower effective viscosity than the standard k-ε model, as shown in figures (6, a & b) while SST k-ω model [16] predicts low dissipation when compared with other models.

While the k-ω models did not have a production term in the transport equation for dissipation rate. The balance between the production and dissipation of *k* affects the turbulent viscosity, which is dominant in the diffusion term.

8-Distribution of turbulent viscosity

The turbulent viscosity μ_t is directly related to the Reynolds stresses, and hence its model is a vital part of any RANS based turbulence model. The turbulent viscosity signifies the resistance offered to the flow due to turbulent mixing. The standard k-ω model given by [17] shows interestingly highest values of μ_t at the leading edge region. These results are the turbulent mixing process taking place in these regions, thus having increased diffusion. The realizable k- ε model produces a maximum turbulent viscosity for both suction and upper sides as compared to other models, while SST k-ω model predicts the minimum values of μ_t, as shown in figures (7, a & b).

9-Distribution of strain rate

Strain rate is the second invariant of the strain rate tensor, relates the shear stress with viscosity. The turbulent stresses are found to increase as the mean rate of deformation or strain rate increases. Thus, the strain rate tensor is one of the important components of the turbulence model, especially the models based on Boussinesq approximation. The strain rate *S* as given by [18] is defined by:

$$S_{ij} = \frac{1}{2}\left(\frac{\partial u_j}{\partial xi} + \frac{\partial u_i}{\partial x_j}\right) \quad (6)$$

The distribution of strain rates are shown in figures (7, a & b). All models estimate high strain rate at the leading and trailing regions. The SST k-ω model predicts high strain rates on the upper side when compared with other models.

10-Turbulencemodels analysis

Based on the analysis of the numerical results compared with the experimental measurements, the general observation about the accuracy of different turbulence examined.

In the original form of the Spalart-Allmaras model, it is effectively a low-Reynolds-number model, requiring the viscous-affected region of the boundary layer to be properly resolved. This might be why make the model less sensitive to numerical error when non-layered meshes are used near the walls [19]. However, this model shows good C_p distributions close to the experimental measurements. The k-ε model does not accurately predict the pressure coefficients distribution. The turbulence kinetic energy and the dissipation rate were quite high The RNG k-

ε model is the modified form derived from the standard k-ε model using the statistical technique called a renormalization group theory. It has an additional term in the transport equation for ε, which reportedly improves the accuracy of the model for highly strained and swirling flows. This required a suitable treatment near wall region._Orzag [15] one of the originators of the RNG model, stated that the reduction in the value of the constants in the RNG theory reduced the rate production of *k* and dissipation. Thus, as reported by [20], the model actually predicts lower effective viscosity. This is evident from the results obtained in this study as the RNG k-ε model estimates low values of *k*, ε, and μ_t, as shown in figures ((4, 5, 6, 7 and 8). One of the important features of the RNG k-ε model is the strain dependant term presents in the transport equation for ε. This term tweaks the dissipation rate in highly strained regions of the flow and reduces it in low strained regions. One more variant of the k- ε model is the realizable k- ε model. It features a formulation of the turbulent viscosity and a transport equation for ε, derived from an exact equation for the transport of the mean-square vortices fluctuation. This model is consistent the physics of the turbulent flows, satisfying some constraints on the Reynolds stresses, and thus called realizable. With these modifications, the realizable k- ε performs better C_p distributions when compared with standard k- ε model and shows very close RNG k- ε C_p distributions, as shown in figure (2). The distribution of *k* for this model is similar to that of RNG k-ε model, with the same trend for the dissipation rate, as shown in figures (6). In terms of the values of strain rates, this model falls among the other models for most regions, as shown in figures (8). This model predicts high turbulent viscosities when compared with other models, as shown in figures (7).

Similar to the k- ε model, the standard k-ω model is a two-equation model based on the isotropic eddy viscosity concept. Instead of using the transport equation for the turbulence dissipation rate ε, this model solves the transport equation for the specific dissipation rate ω. Unlike the standard k-ε model, this model has not been tested extensively for applicability to the boundary layer flows around the turbine blade. At the present, this model predicts highest values of *k*, ε, μ_t , and *S* at the leading edge region when compared with the other models, as shown in figures ((4, 5, & 6). This model is not succeeded to be accurate with respect to $C_p$values.

The blend of capability of the standard k-ω model to handle low-Reynolds number effects and the far-field performance of the k- ε model is the SST k-ω model. In transforming the k- ε model in the formulation of k-ω model, this model multiplies both the formulations with a blending function which "activates" the k-ω model in the near wall region and uses the k- ε model in the far field region. It involves a modified definition of the turbulent viscosity in order to account for the transport of the turbulent shear stresses.

11- Accuracy of solution

As seen from the predicted results, when the CFD code predicts the flow separation, the problem became so complicated, so that it leads to increase the number of iterations to convergence. According to this concept and with regards to the number of iterations to convergence, the model RNG k-ε exhibits minimum number of iterations to convergence (371), i.e. CFD code early predict the flow separation, while SST k-ω exhibits maximum number of iterations to convergence (928).

12-Conclusions

Using k-ε turbulence model in the computations overestimate the turbulence kinetic energies, especially in the regions of high velocity at suction side and not accurately predict the flow separation on the blade suction side.

RNG k-e turbulence model gave the closes prediction of pressure distribution when compared with the experimental data and exhibits minimum number of iterations to convergence of (371).

R k- ε turbulence model predicts acceptable closeness to the experimental pressure distribution.

Prediction of standard k-ε (S k-ε) and standard k-ω (Sω-ε) turbulence models variants are not in a good agreement with the experimental data, in which the percentage disagreement between (S k-ε) maximum predicted values of C_p on blade suction side at (x/c) = 0.45 and the experimental values of C_p was 13.8%, while for (S ω-ε) it showed a maximum values of 19.4% at the same (x/c) on suction side. Thus these two turbulence models fail to predict accurately C_p distribution. One of the reasons for this discrepancy may be due to use the isotropic eddy viscosity concept, which leads to predict highly anisotropic flow properties encountered in these situations.

The SST k-ω turbulence model predicts high strain rates on the suction side when compared with other models, minimum values of μ_t, low dissipation when compared with other models, and considerably low *k* values for both the suction and pressure blade sides due to the slow growth of shear stresses. The SST k-ω turbulence

model also predicts the most negative pressure coefficients and exhibits maximum number of iterations to convergence of (928).

List of symbols

C_p: Coefficient of pressure

C_μ: Constants in two-equation turbulence models

I: Turbulence intensity

k: Turbulent kinetic energy, m^2/s^2

L_C: Characteristic length, m

s: Cascade pitch, m

S: Rate of strain tensor, 1/ s

R_ε: Extra term for turbulence dissipation rate in RNG k-ε model

u: Velocity component in x-directions *m/s*

x & y; Coordinate direction

β; Coefficients in k-ω models

ε: Dissipation rate of turbulent kinetic energy, m^2/s^3

μ_t: Turbulent viscosity, N/m^2s

μ_τ: Turbulent eddy viscosity, N/m^2s

$\tilde{v}$: Working variable for the turbulence model ,m^2/s

P: Density ,m^3/s

Ω: Specific dissipation rate, *1/s*

η & η_o: constants in RNG k-ε model

References

[1] Jesse, Wells, "Effects of Turbulence Modeling on RANS Simulations of Tip Vortices", M.Sc. Thesis, Virginia Polytechnic Institute and State University, Engineering Mechanics, August 3, 2009.

[2] Chang-Hsien, Tai, Ding-San, Wang, Ping-Hei, Chen, Uzu-Kuei, Hsu, and Jr-Ming, Miao, "Numerical Studies of the Passage Flowfield in a 3-D Transonic Turbine Blade Cascade**"**, The Chinese Journal of Mechanics, Vol.17, No.4, December 2001.

[3] Ümit, Sönmez and Mustafa, Tutar, "Computational Modelling of Turbulent Flow in a Transonic Linear Turbine", Department of Mechanical Engineering, Mersin University, pp.1-11, 2003.

[4] A. Yangyozov and R. Willinger, "Calculation of Flow Characteristics in Heat Turbomachinery Turbine Stage with Different Three Dimensional Shape of the Stator Blade with Ansys CFX Software", DIProjektbericht, ZID: 08-302-4, 2005.

[5] Johan, Hjärne, Valery, Chernoray, Jonas, Larsson, and Lennart, Löfdahl,

"Numerical Validations of Secondary Flows and Loss Development Downstream of a Highly Loaded Low Pressure Turbine Outlet Guide Vane Cascade", ASME Turbo Expo, May 14-17, 2007, Montreal, Canada, 2007.

[6] W. B. de Wolf, S. Woldendorp and T. Tinga, "Analysis of Combined Convective and Film Cooling on an Existing Turbine Blade", National Aerospace Laboratory NLR, RTO-AVT Symposium on Heat Transfer and Cooling in Propulsion and Power Systems, Loen, Norway, May 2001.

[7] Maskel, C.E., "A theory of Blockage Effects on Bluff Bodies and Stalled Wings in a Closed Wind Tunnel", ARC R & M 3400, 1965.

[8] Launder B. E., Spalding D. B., "The Numerical Computation of Turbulent Flows", Computer Methods in Applied Mechanics and Engineering, Vol. 3, pp. 269-289, and 1974.

[9] Davidson, L., "An Introduction to Turbulence Models", Chalmers University of Technology, Department of Thermo and Fluid Dynamics, 2003.

[10] Canelli, C., Sacchetti, M., and Traverso, S., "Numerical 3-D Conjugate Flow and Heat Transfer Investigation of a Convection-Cooled Gas Turbine Vane", ATI-NASA, 2003

[11] Versteeg**, H. K., and Malalasekera, W.,** "An Introduction to Computational Fluid Dynamics-The Finite Volume Method", Longman Group Ltd., 1995.

[12] Canelli**, C., Sacchetti, M., and Traverso, S.,** "Numerical 3-D Conjugate Flow and Heat Transfer Investigation of a Convection-Cooled Gas Turbine Vane", ATI-NASA, 2003.

[13] **Yang, Z. and Shih, T.H.,** "New time scale based k - e model for near – wall turbulence", *AIAA*, J.31 (7), 1191-1197, 1993.

[14] **Shih T. H., Liou W. W., Shabbir A. and Zhu J.,** "A New k-ε Eddy-Viscosity Model for High Reynolds Number Turbulent Flows - Model Development and Validation", Computers Fluids, Vol. 24, No. 3, pp. 227-238, 1995.

[15] Yakhot V., and Orszag S.A., "Renormalization Group Analysis of Turbulence, I - Basic Theory", Journal of Scientific Computing, Vol. 1, No. 1, pp. 3-51, 1986.

[16] Menter F. R., "Two-equation Eddy-viscosity Turbulence Models for Engineering Applications", AIAA Journal, Vol. 32, No. 8, pp.1598¬1605, 1994.

[17] Wilcox **D. C.,** "Turbulence Modeling for CFD", Second

Edition, DCW Industries, Inc., 2002.

[18] J. Dacles-Mariani, G. G. Zilliac**, J. S. Chow, and P. Bradshaw,** "Numerical/ Experimental Study of a Wingtip Vortex in the Near Field", AIAA Journal, 33(9), pp.1561-1568, 1995.

[19] **You, Qin, Wang, Peter, Jackson and Josef, Ackerman** "Numerical Investigation of Turbulence Model", Computational Fluid Dynamics Journal, pp.198-205, April 2006 .

Flow over a Sphere Using LES and the Spalart-Allmaras

[20] **Easom G. J.,** "Improved Turbulence Models for Computational Wind Engineering", Ph.D. Thesis in Civil Engineering, University of Nottingham, UK., 2000.

Table (1)

Number of blades		5
Chord	[mm]	135
Axial chord	[mm]	123.32
Blade stagger angle	[°]	24
Pitch	[mm]	135
Span	[mm]	200
Inlet flow angle	[°]	40
Blade inlet and outlet angles respectively	[°]	42.7, 60
Solidity		1

Figure (1) cascade blade inthe wind tunnel test section.

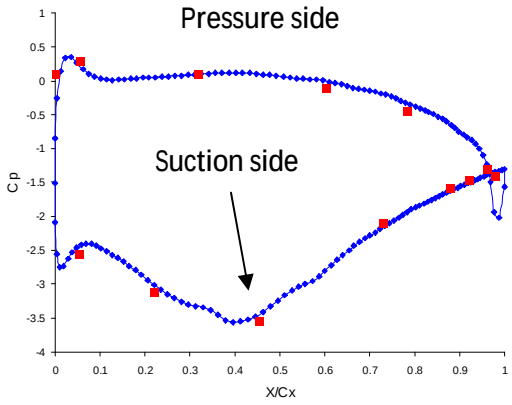

— S-A model and ■ Experiment

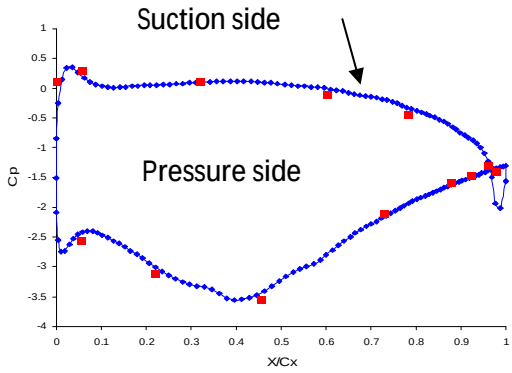

— S k-ε model and ■ Experiment

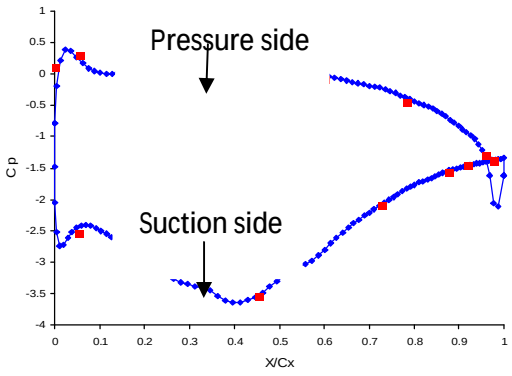

— RNG k-ε model, ■ Experiment

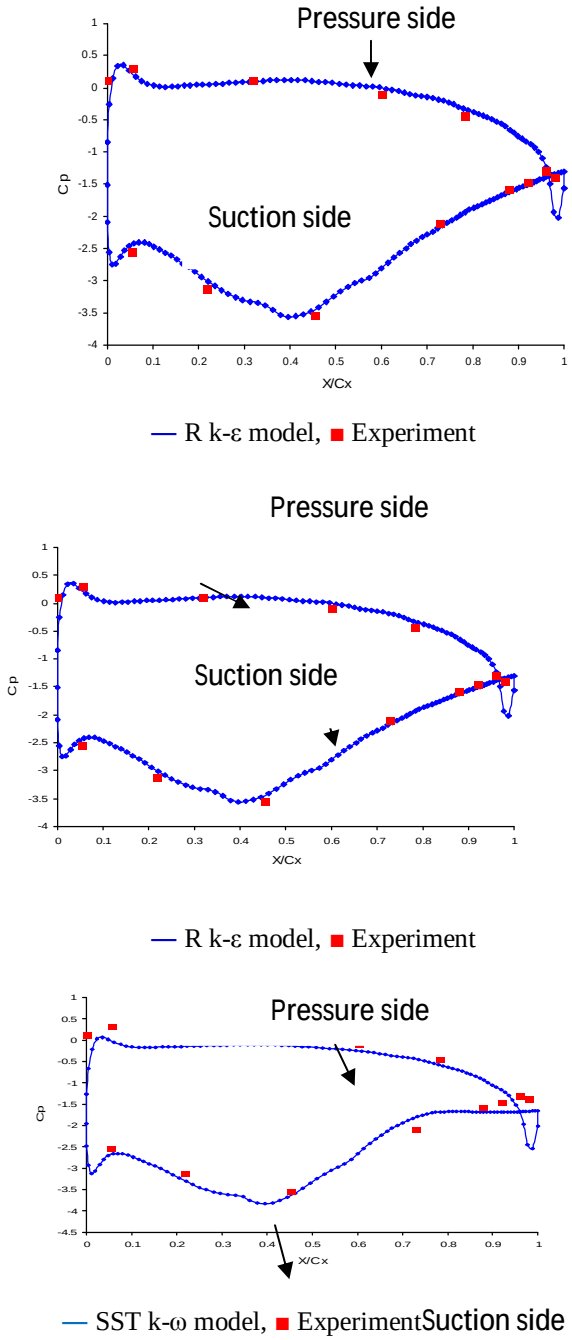

Figure (2) Comparison of C_p distributions between the experimental and CFD results

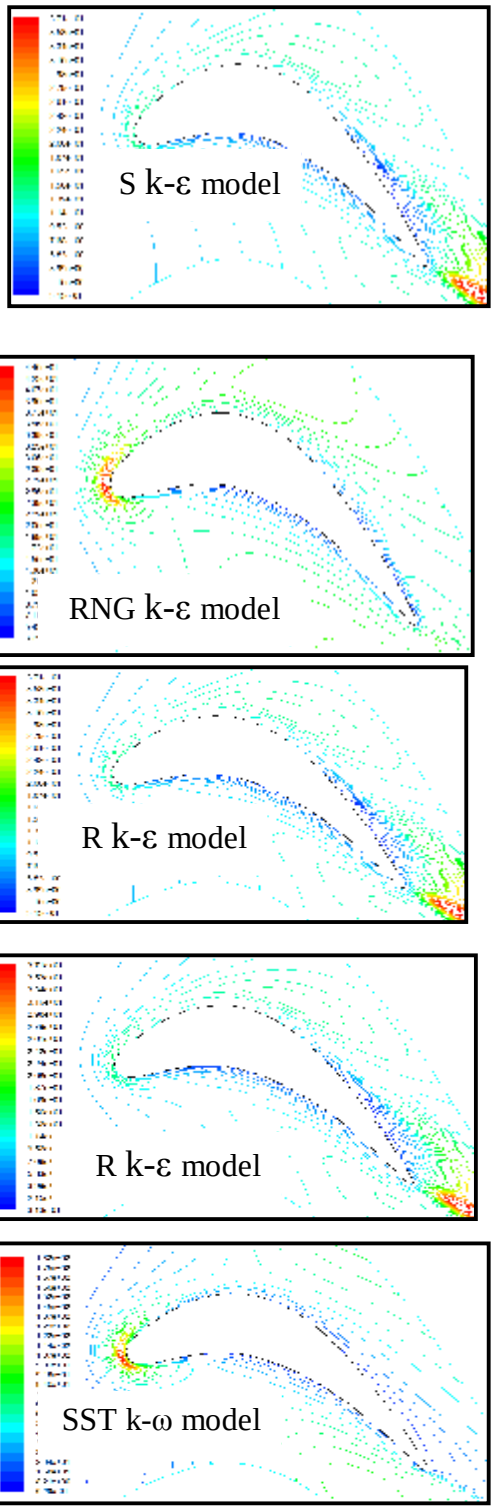

Figure (3) Distribution of turbulent kinetic energy contours around turbine blade

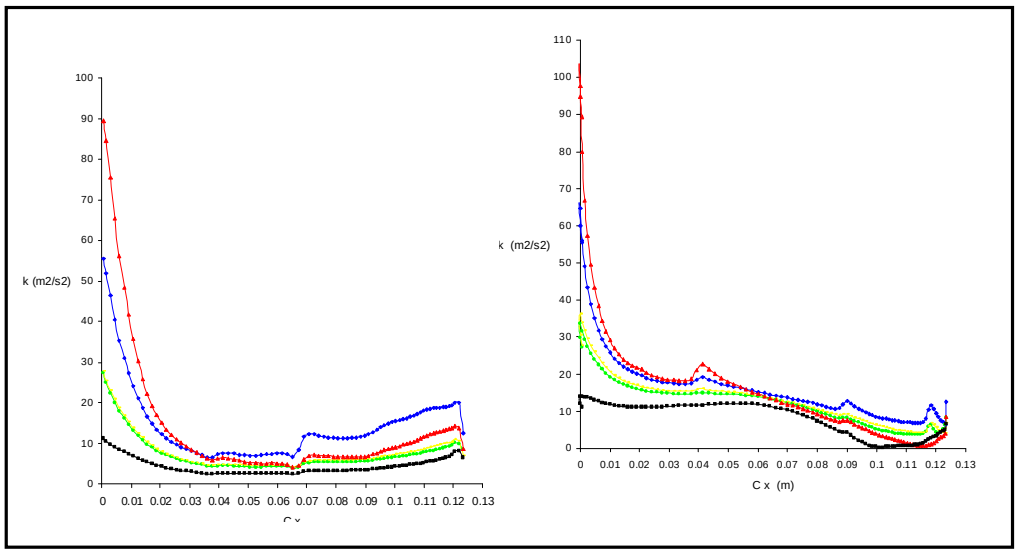

Figure (4) Turbulent kinetic energy distributions along blade pressure and suction sides

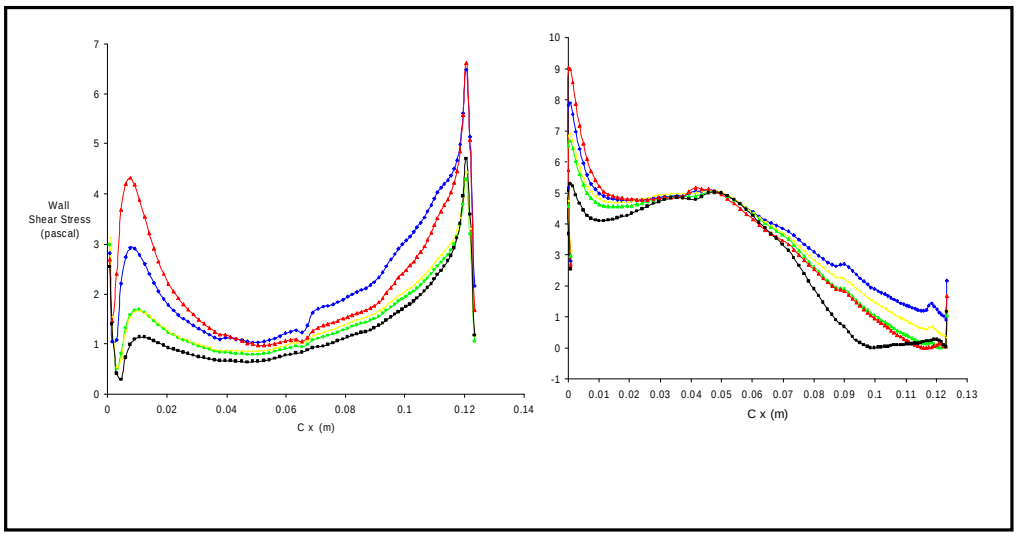

Figure (5) Wall shear stress distributions along blade pressure and suction sides

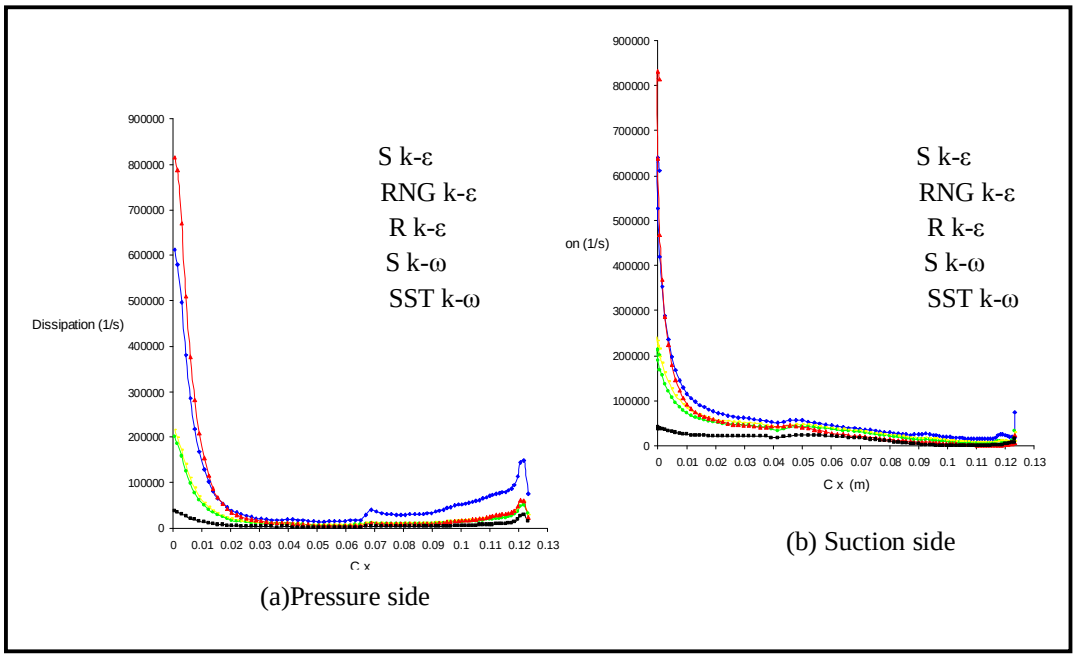

(a)Pressure side (b) Suction side

Figure (6) Dissipation rate distributions along blade pressure and suction sides suction side

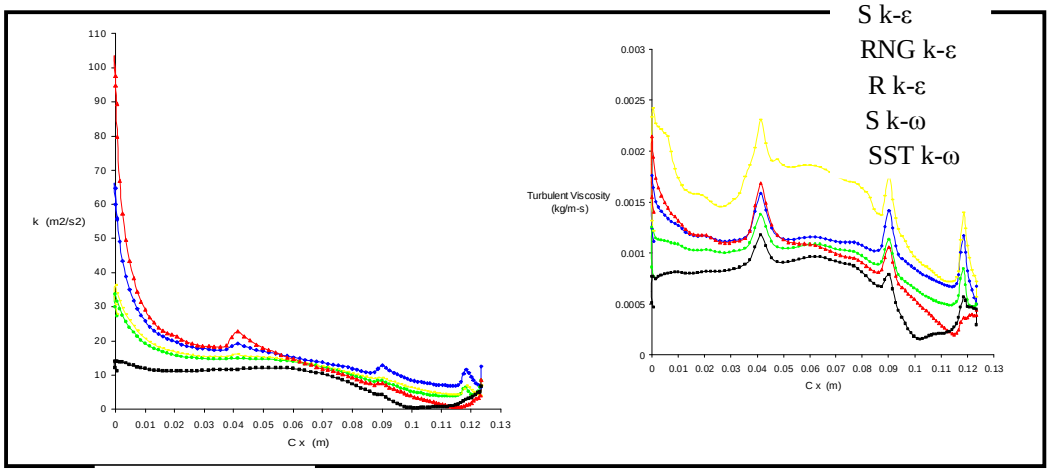

(a)Pressure side (b) Suction side

Figure (7) Turbulent viscosity distributions along blade pressure and suction sides suction side

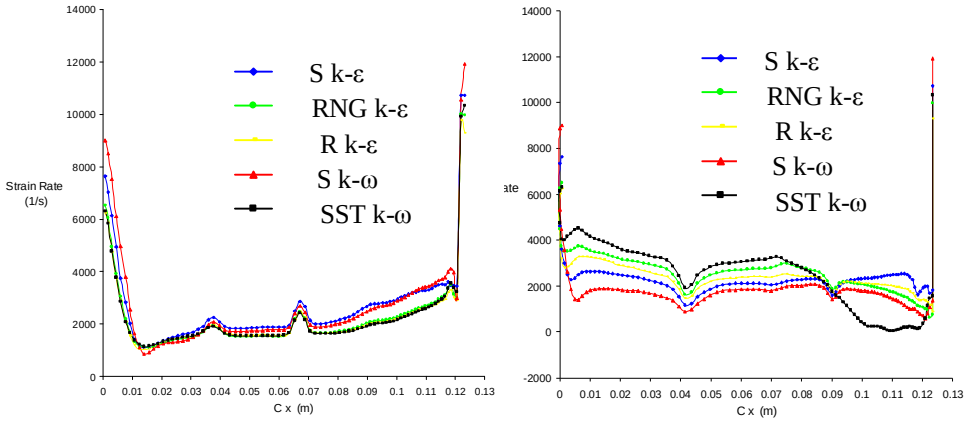

(a)Pressure side (b) Suction side

Figure (8) Strain rate distributions along blade pressure and suction sides